

### **Supporting information:**

### **Experimental Section**

**Synthesis of CdS nanorods:** CdS nanorods (CdS-NRs) was prepared by heat treatment of the mixed solution of Cd(NO<sub>3</sub>)<sub>2</sub> and thiourea using ethylenediamine as solvent. Typically, 3.8 g of Cd(NO<sub>3</sub>)<sub>2</sub>•2H<sub>2</sub>O and 2.8 g of thiourea were added into a conical flask containing 64 ml of ethylenediamine. After magnetic stirring for 1 h, the mixed solution was transferred to a 100 ml Teflon-lined autoclave, and followed by heat treatment at 180 °C for 48 h. After cooling down to room temperature, the precipitates were filtrated through a membrane filter (pore size: 0.45 μm) and thoroughly rinsed with ethanol and distilled water until the pH of the filtrate was ~ 7. The obtained cake was then moved into an oven for drying at 60 °C for 10 h. About 2.0 g of CdS-NRs can be obtained with a yield of 98%.

**Metallic Bi modified CdS-NRs:** Metallic Bi was *in-situ* deposited on the surface of CdS-NRs by reduction of Bi(NO<sub>3</sub>)<sub>3</sub>•5H<sub>2</sub>O. Typically, 1.16 g of Bi(NO<sub>3</sub>)<sub>3</sub>•5H<sub>2</sub>O was firstly dissolved in 50 ml of ethylene glycol solution (50 v/v%). Then 1.0 g of the synthesized CdS-NRs was also added into the mixed solution under magnetic stirring, which was kept at 80 °C for 1 h. After cooling down to room temperature, the precipitates were washed with methanol and distilled water. The precipitates were dispersed in 50 ml of NaBH<sub>4</sub> solution (1.0 molL<sup>-1</sup>). After reaction for 4 h under magnetic stirring, the resulted powders were washed with water and methanol for several times, and dried at 60 °C for 6 h. As the calculated weight ratio of Bi to CdS is 50%, the obtained sample is named as S50.

For comparison, a series of Bi/CdS-NRs photocatalysts were prepared under other identical conditions except the amount of Bi(NO<sub>3</sub>)<sub>3</sub>•5H<sub>2</sub>O (Table S1). The samples were named as Sx, where x represents the weight ratio of Bi to CdS (wt. %).

**Characterization:** X-ray diffraction (XRD) patterns were recorded on an X-ray diffractometer (D8 ADVANCE, Bruker) using Cu Kα radiation source ( $\lambda = 1.54056 \text{ \AA}$ ) at a scan rate of 5° min<sup>-1</sup>. The

morphologies of the samples were observed on field emission scanning electron microscopy (FESEM, SU8010, Hitachi) and a Tecnai G20 electron microscope (TEM). Energy dispersive X-ray spectroscopy (EDS) mapping were implemented by a Thermo Scientific Talos F200S scanning/transmission electron microscope to observe the microstructure and the element distribution of the samples. Nitrogen sorption-desorption isotherms were performed in a Micromeritics ASAP 2020 nitrogen adsorption apparatus. X-ray photoelectron spectroscopy (XPS) measurements were done in a Kratos XSAM800 XPS system. Powder UV-visible absorption spectrum was recorded on a UV-2550 spectrophotometer using BaSO<sub>4</sub> as a reflectance standard. The photoluminescence (PL) spectrum of the photocatalyst was recorded on a on an F-7000 Fluorescence Spectrophotometer ( $\lambda_{\text{ex}} = 330 \text{ nm}$ ). Electron spin-resonance (ESR) spectroscopy measurement was obtained from JES-FA 200 EPR spectrometer in DMPO solution under visible irradiation. Kelvin probe apparatus (Instytut Fotonowy, Poland) was used to detect the surface work function (W), which was monitored using an LED lamp as the light source in conjunction with a monochromator.

***(Photo)electrochemical measurement:*** Photocurrent and electrochemical impedance spectroscopy (EIS) were measured on a three-electrode system in CHI760E electrochemical workstation. CdS electrodes were prepared as follows: Firstly, 20 mg of the photocatalyst was dispersed in 1.0 ml of alcohol solution (volume ratio of ethanol and water was 1:1). After ultrasonicated for 30 min, 30  $\mu\text{l}$  of naphthol was also added. The resulted slurry was then coated on an indium-tin oxide (ITO) glass electrode by a doctor-blade method. The ITO/CdS electrode, Pt plate, and Ag/AgCl electrode were used as the working, counter, and reference electrodes, respectively. Na<sub>2</sub>SO<sub>4</sub> solution (0.4 mol L<sup>-1</sup>) was used as electrolyte solution. In photocurrent measurement, an LED lamp (3 W) emitted mainly at  $\lambda = 420 \pm 10 \text{ nm}$  was used as the light source. EIS was measured under open circuit potential with the frequency of 0.1~1000 Hz. Mott-Schottky measurement was carried out under direct current potential polarization at different fixed frequency of 1000 Hz.

### ***Evaluation of the photocatalytic activity.***

Photocatalytic oxidation of NO was carried out in a continuous-flow reactor (4.5 L) with an LED lamp ( $\lambda > 420$  nm) as the light source that simulates sunlight (set-up see Fig. S1). Briefly, 0.02 g of the photocatalyst was dispersed into 30 mL of deionized water to form suspensions. After ultrasonication for 10 min, the suspensions were transferred into a culture dish (11 cm of diameter) and heated at 60 °C for 12 h for evaporation. The obtained photocatalyst film was put into the photochemical reactor. Before irradiation, NO and air were mixed in a bottle, while the concentration of NO was adjusted by a mass flow controllers. After reaching NO adsorption-desorption equilibrium (about 550 ppb), the photocatalytic reaction begins as soon as the LED lamp is turned on. The concentrations of NO and the accompanying NO<sub>2</sub> were detected online at the exit of the reactor by a chemiluminescence NO<sub>x</sub> analyzer (Advanced Pollution Instrumentation, Teledyne Technologies, USA).

***In-situ DRIFTS analysis:*** In-situ DRIFTS were performed on a Tensor II FT-IR spectrometer (Bruker) equipped with a reaction chamber. Before adsorption and photocatalytic oxidation of NO, the chamber was cleaned by purging with high purity He gas. Then, the mixed gases of NO (100 ppm balanced in N<sub>2</sub> gas) and O<sub>2</sub> were introduced into the reaction chamber with a flow rate of 50 ml min<sup>-1</sup> for each. A visible LED lamp is used as the light source to initiate photocatalytic oxidation of NO over S50 photocatalyst.

**Table S1.** Physical property of the photocatalyst.

Sample	Starting materials		Bi/CdS <sup>a</sup> (wt.%)	nitrogen sorption results		
	CdS (g)	Bi(NO <sub>3</sub> ) <sub>3</sub> •5H <sub>2</sub> O (g)		S <sub>BET</sub> <sup>b</sup> (m <sup>2</sup> g <sup>-1</sup> )	PV <sup>c</sup> (cm <sup>3</sup> g <sup>-1</sup> )	APS <sup>d</sup> (nm)
CdS	-	-	-	28.6	0.15	21.4
S10	1.0	0.23	10	24.2	0.12	19.9
S20	1.0	0.46	20	21.8	0.14	25.9
S50	1.0	1.16	50	19.2	0.11	23.1
S100	1.0	2.32	100	18.2	0.13	29.0
S150	1.0	3.48	150	8.8	0.08	39.4
S200	1.0	4.64	200	1.2	0.02	60.9

<sup>a</sup>Calculated weight ratio of Bi to CdS from the starting materials.

<sup>b</sup>Brunauer-Emmett-Teller (BET) surface area of the photocatalyst is determined by the multipoint BET method using the adsorption data in the relative pressure ( $P/P_0$ ) range from 0.05 to 0.3.

<sup>c</sup>Pore volume (PV) is determined from the adsorption branch of the nitrogen isotherms at  $P/P_0 = 0.994$ .

<sup>d</sup>Average pore size (APS) is estimated from the adsorption branch of the nitrogen isotherms using the BJH method.

**Table S2.** Photocatalytic oxidation of NO over difference photocatalyst.

Photocatalyst	Reaction conditions	NO removal rate (%)	Reference
blue TiO <sub>2</sub> with OV <sub>s</sub>	Xenon lamp ( $\lambda > 400$ nm)	63%	[1]
Fe <sub>1</sub> /TiO <sub>2</sub> -HMS <sub>s</sub>	LED lamp ( $\lambda > 400$ nm)	48%	[2]
g-C <sub>3</sub> N <sub>4</sub> /TiO <sub>2</sub>	visible light	38%	[3]
OV <sub>s</sub> -mediated TiO <sub>2</sub>	visible light (450 W Hg lamp)	41%	[4]
Bi@Bi <sub>2</sub> O <sub>3</sub>	visible light ( $\lambda > 420$ nm)	41%	[5]
SrCO <sub>3</sub> @BiOI	visible light (420-700 nm)	48%	[6]
Pd/C <sub>3</sub> N <sub>4</sub>	halogen lamp (150 W)	52%	[7]
Ti <sub>3</sub> C <sub>2</sub> /g-C <sub>3</sub> N <sub>4</sub>	visible light ( $\lambda > 420$ nm)	57%	[8]

**Table S3.** The calculation of work functions of CdS-NRs, metallic Bi and Bi/CdS-NRs.

Sample <sup>a</sup>	CdS-NRs	Bi	Bi/CdS-NRs
CPD (mV)	107.8	303.4	98.4
$W_{\text{sample}}$ (eV)	4.1422	4.5534	4.3484
$E_{f, \text{vac}}$ (eV)	-4.1422	-4.5534	-4.3484
$E_{f, \text{pH0}}$ (eV)	-0.3578	0.0534	-0.1516
$E_{f, \text{pH7}}$ (eV)	-0.7708	-0.3596	-0.5646

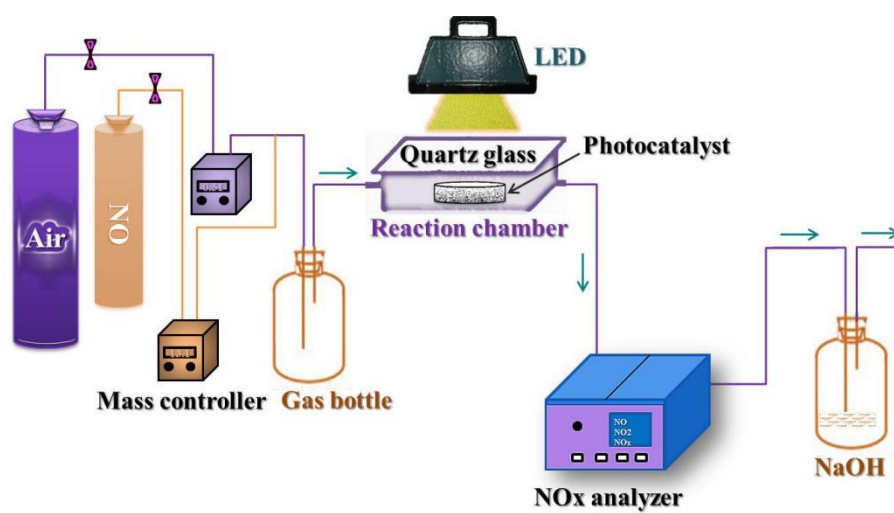


**Fig. S1.** Experimental set-up for the photocatalytic oxidation of NO in a continuous flow reactor.

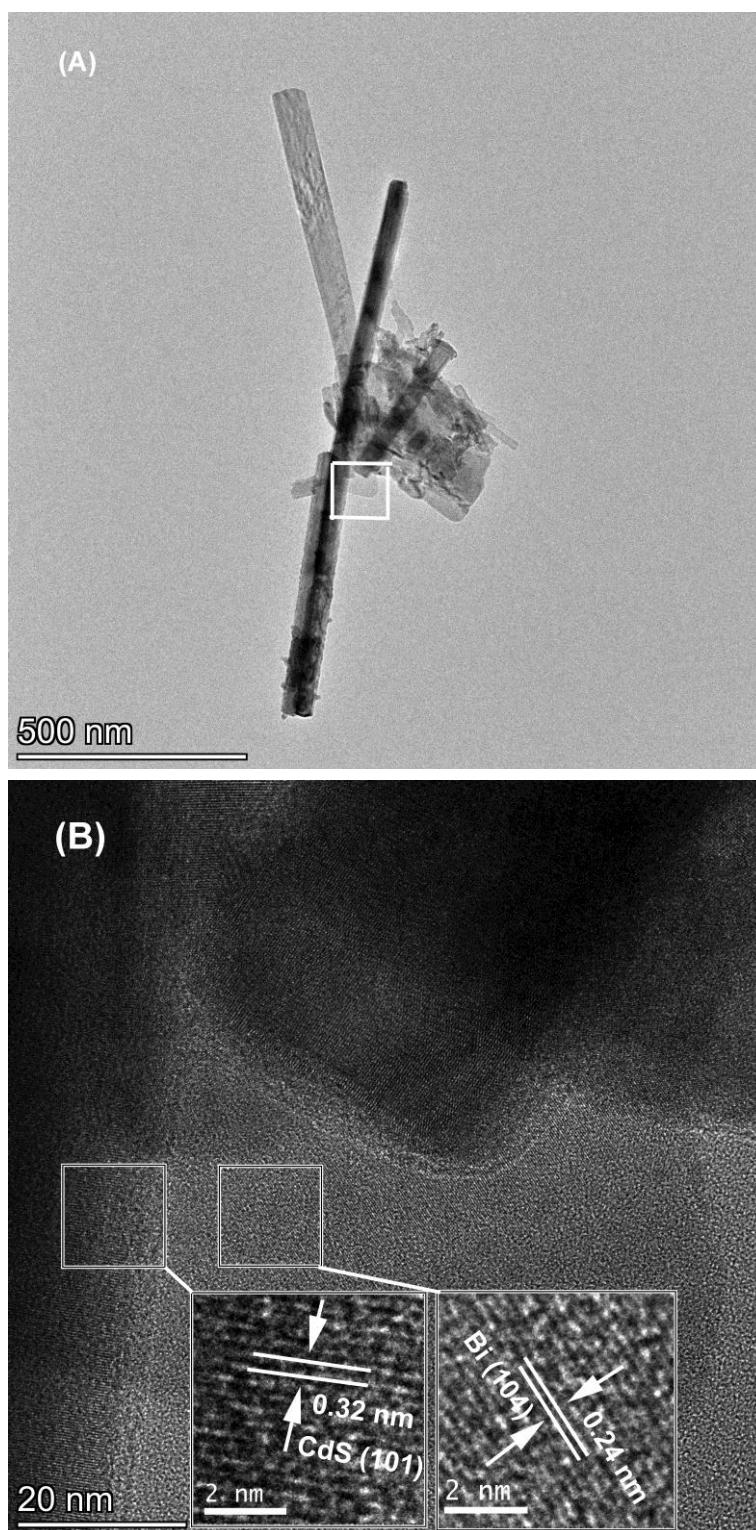


**Fig. S2** TEM (A) and high resolution TEM (B) images of Bi/CdS-NRs sample.

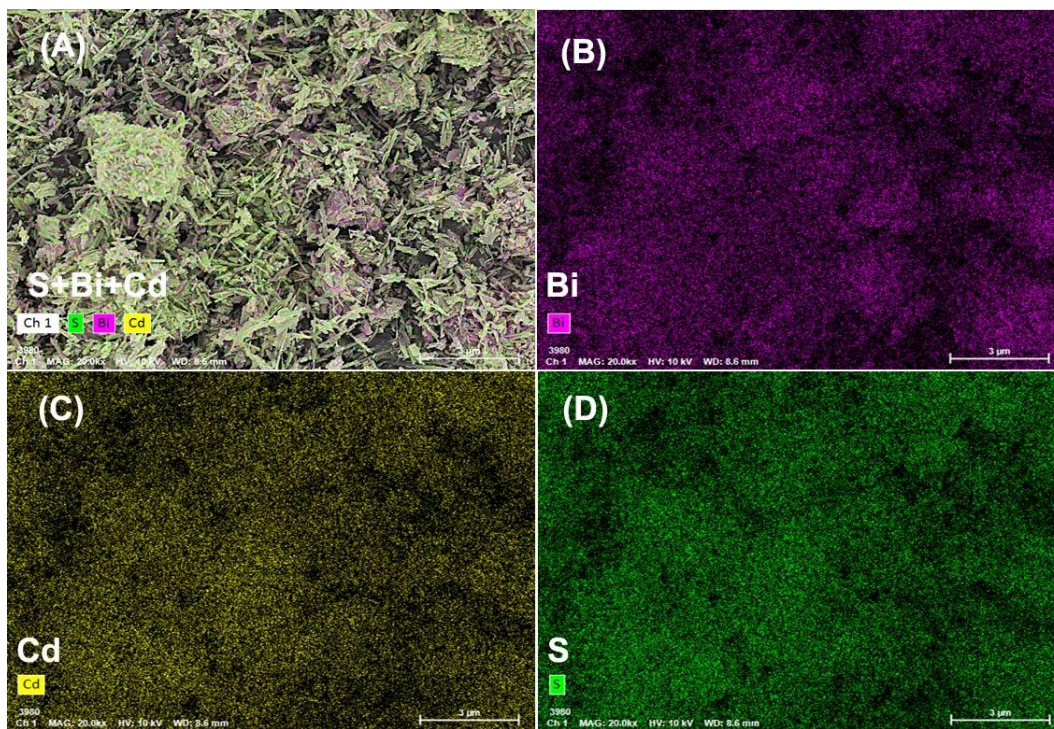
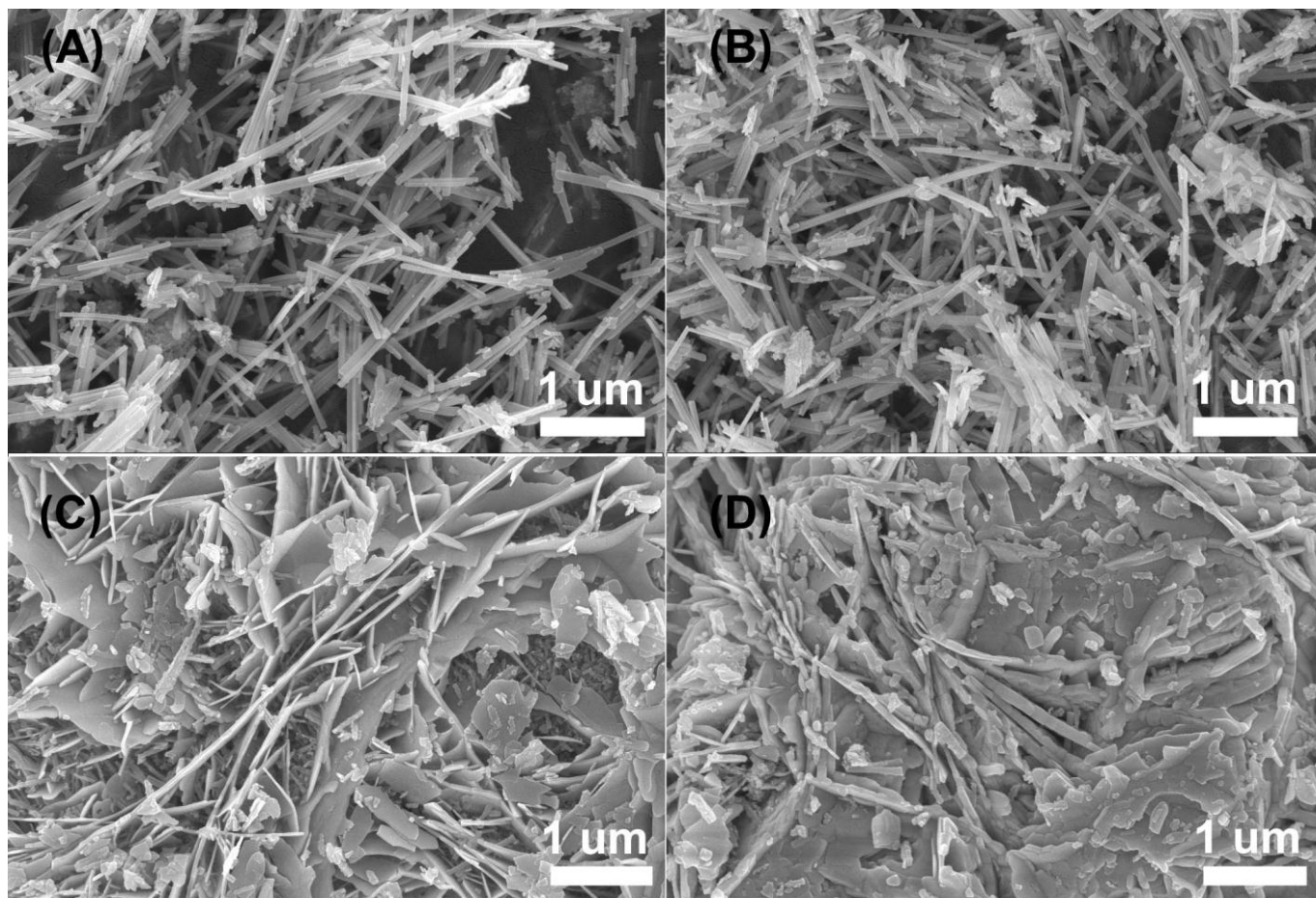
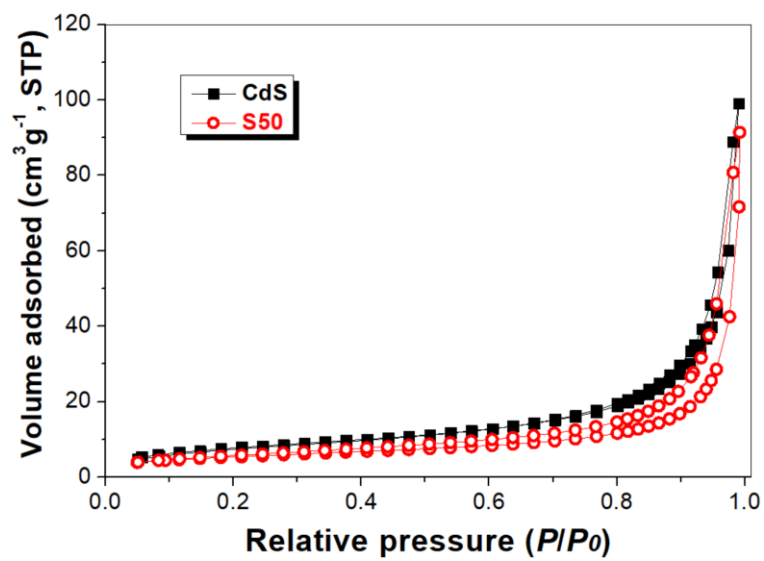


Fig. S3 Element mapping of Bi/CdS-NRs photocatalyst (S50 sample) from SEM image.



**Fig. S4** SEM images of S10 (A), S20 (B), S100 (C) and S150 (D) samples.



**Fig. S5.** Nitrogen sorption-desorption isotherms of CdS-NRs before and after depositing metallic Bi (S50 sample).

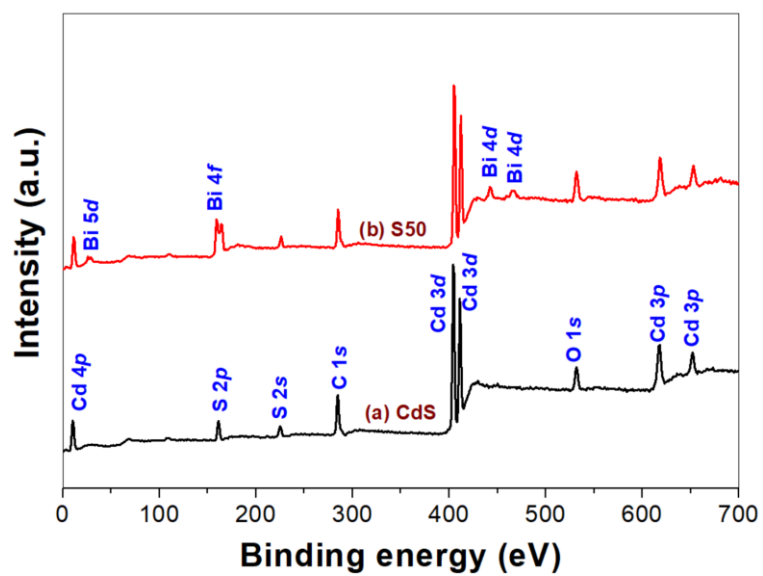


**Fig. S6.** XPS survey spectra of pristine CdS-NRs (a) and Bi/CdS-NRs (b).

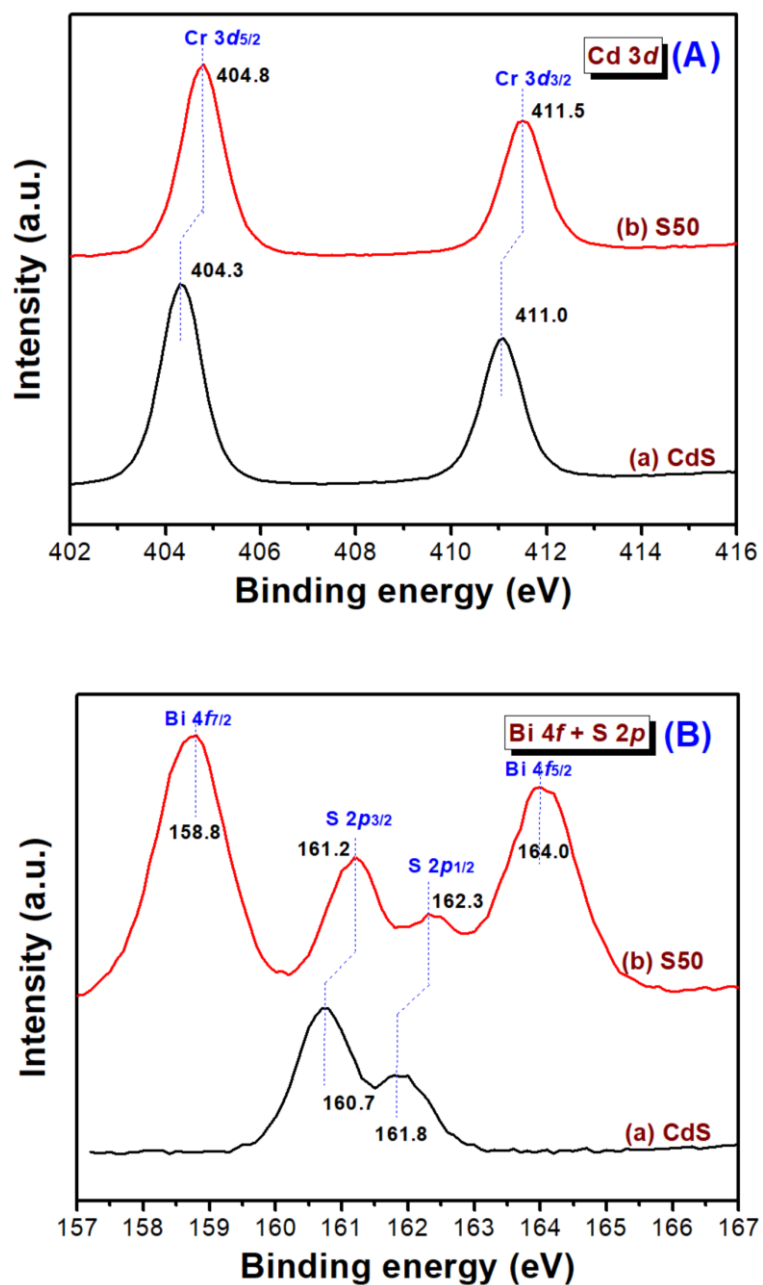


**Fig. S7.** High resolution XPS spectra of pristine CdS-NRs and Bi/CdS-NRs samples in Cd 3d (A) and Bi 4f (B) regions, respectively.

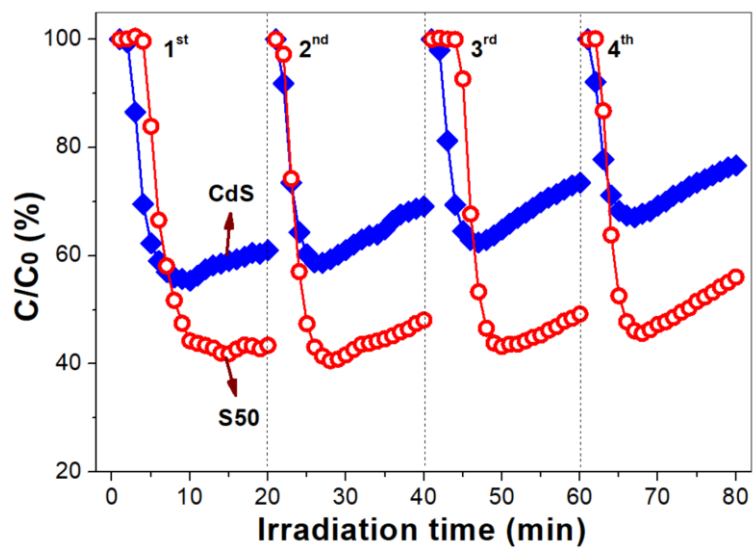


**Fig. S8.** Recycling use of pristine CdS-NRs and Bi/CdS-NRs (S50 sample) for photocatalytic NO oxidation.

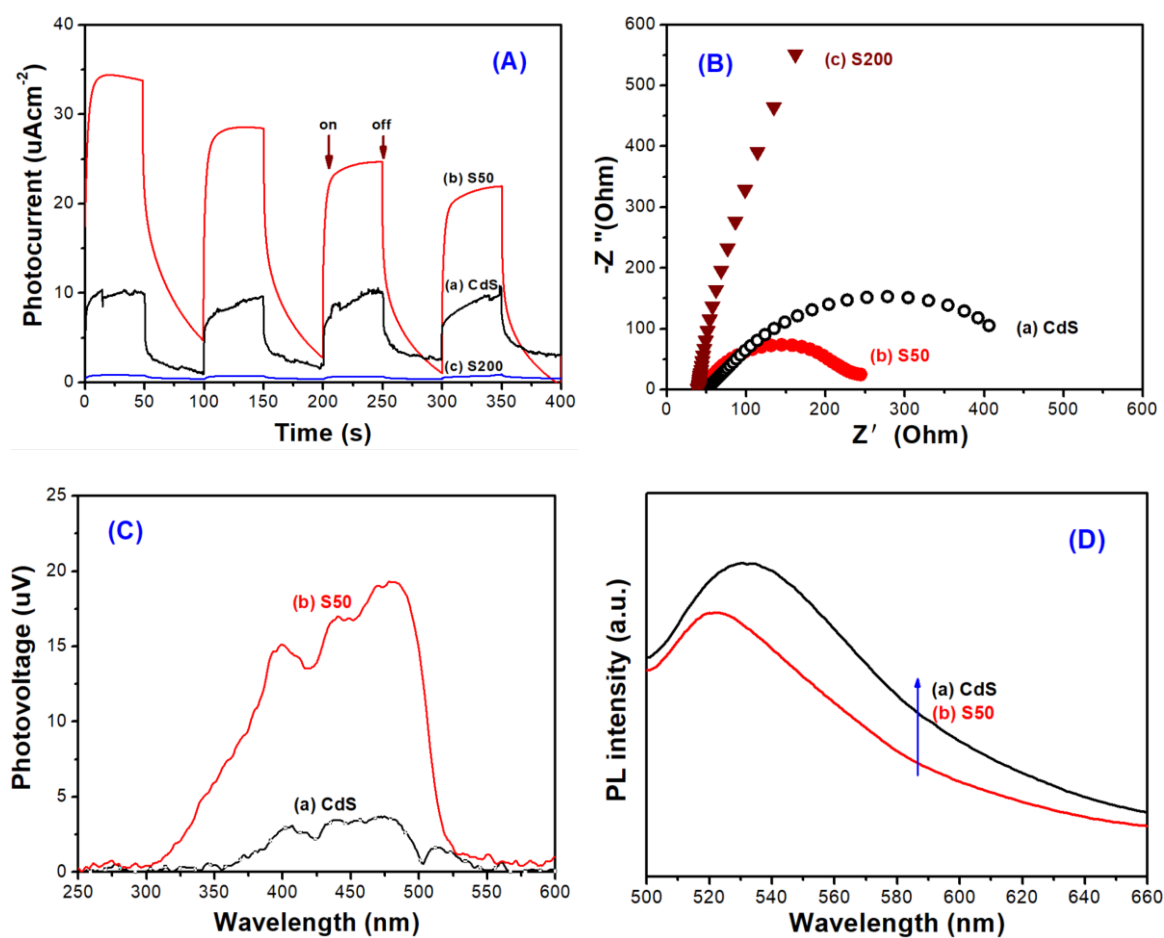


**Fig. S9.** Comparing the photocurrent (A), electrochemical impedance spectroscopy (B), surface photovoltage spectrum (C) and photoluminescence spectrum (D) of the CdS-based photoelectrode.

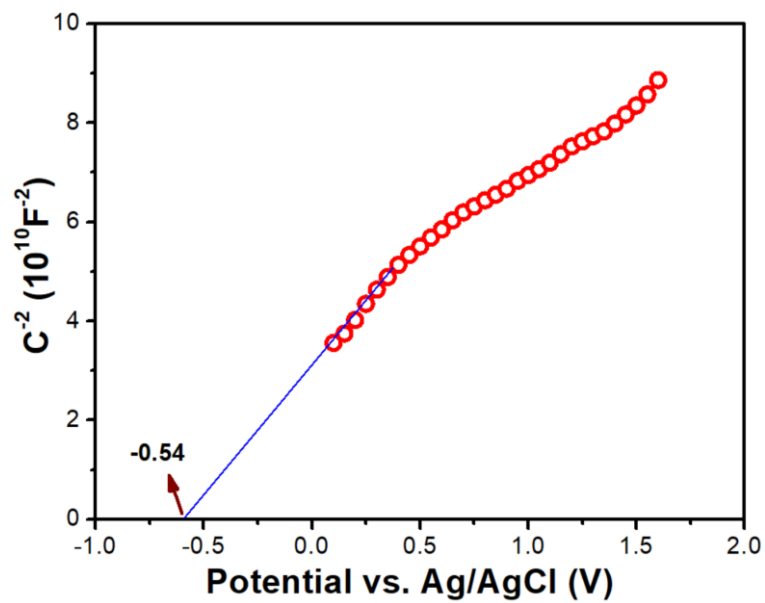


**Fig. S10.** Mott-Schottky plot of pristine CdS-NRs photocatalyst at a fixed frequency of 1000 Hz in  $0.5 \text{ molL}^{-1} \text{ Na}_2\text{SO}_4$  (pH=6.7).

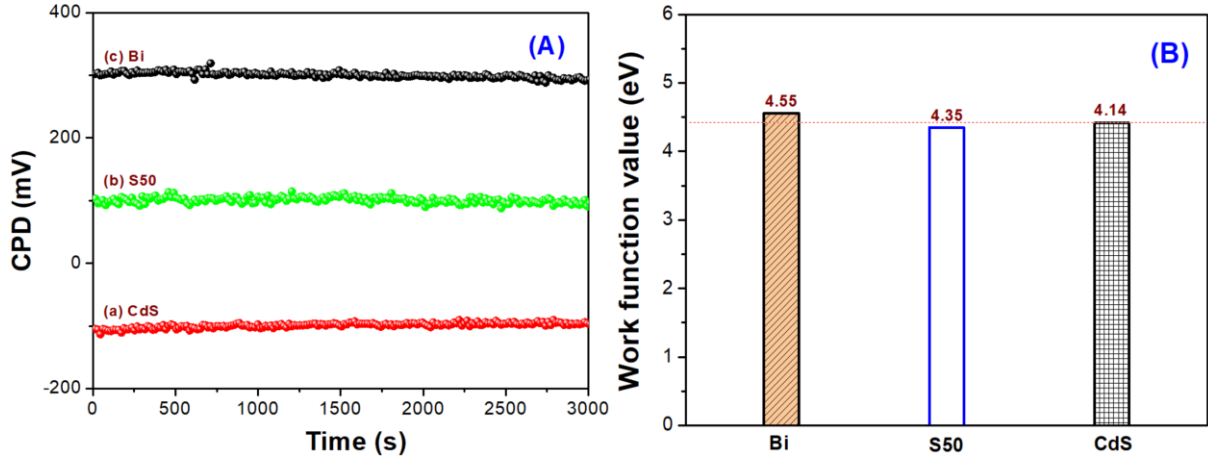


**Fig. S11.** CPD values measured by Kelvin probe (A) and the corresponding work functions (B) of pristine CdS-NRs, Bi/CdS-NRs and metallic Bi, respectively.

Work function ( $W$ ) of sample is calculated by the contact potential difference (CPD) taking a gold mesh as the reference. The calculated equation is  $W_{\text{sample}} = W_{\text{probe}} + e \times \text{CPD}_{\text{sample}}$ , where  $W_{\text{sample}}$ ,  $W_{\text{probe}}$ ,  $e$ , and  $\text{CPD}_{\text{sample}}$  is the work function of a given sample, the work function of gold mesh ( $\approx 4.25$  eV), the electron charge, and the CPD value of the sample, respectively.

Under 365 nm light irradiation, the CPD values of CdS-NRs, metallic Bi, and Bi/CdS-NRs samples are  $-107.8$ ,  $-303.4$ , and  $98.4$  mV, respectively. As a result,  $W$  of CdS-NRs, Bi, and Bi/CdS-NRs samples are  $4.14$ ,  $4.55$ , and  $4.34$  eV, respectively.

According to equation 1

$$E_{f, \text{vac}} = E_{\text{vac}} - W \quad (1)$$

where  $E_{\text{vac}}$  is the energy of a stationary electron at the vacuum level (assumed as 0 eV) and  $E_{f, \text{vac}}$  is the Fermi levels of the samples at the vacuum level, and the conversion formulas (equations 2 and 3),

$$E_{f(\text{vs. NHE, pH0})} = -4.5 \text{ V} - E_{f, \text{vac}} \quad (2)$$

$$E(\text{vs. NHE, pH7}) = E(\text{vs. NHE, pH0}) - 0.059\text{pH} \quad (3)$$

The  $E_f$  of CdS-NRs, Bi, and Bi/CdS-NRs samples is calculated to be  $-0.77$ ,  $-0.36$ , and  $-0.56$  V (vs. NHE at pH = 7), respectively.

## References:

- [1] H. Shang, M. Li, H. Li, S. Huang, C. Mao, Z. Ai, L. Zhang, Oxygen vacancies promoted the selective photocatalytic removal of NO with blue TiO<sub>2</sub> via simultaneous molecular oxygen activation and photogenerated hole annihilation, *Environmental Science & Technology*, 53 (2019) 6444-6453.
- [2] Z. Hu, X. Li, S. Zhang, Q. Li, J. Fan, X. Qu, K. Lv, Fe<sub>1</sub>/TiO<sub>2</sub> hollow microspheres: Fe and Ti dual active sites boosting the photocatalytic oxidation of NO, *Small*, 16 (2020) e2004583.
- [3] T. Giannakopoulou, I. Papailias, N. Todorova, N. Boukos, Y. Liu, J. Yu, C. Trapalis, Tailoring the energy band gap and edges' potentials of g-C<sub>3</sub>N<sub>4</sub>/TiO<sub>2</sub> composite photocatalysts for NO<sub>x</sub> removal, *Chemical Engineering Journal*, 310 (2017) 571-580.
- [4] Z. Gu, Z. Cui, Z. Wang, T. Chen, P. Sun, D. Wen, Reductant-free synthesis of oxygen vacancies-mediated TiO<sub>2</sub> nanocrystals with enhanced photocatalytic NO removal performance: An experimental and DFT study, *Applied Surface Science*, 544 (2021).
- [5] P. Zhang, Y. Huang, Y. Rao, M. Chen, X. Li, W. Ho, S. Lee, J. Cao, Chemical etching fabrication of uniform mesoporous Bi@Bi<sub>2</sub>O<sub>3</sub> nanospheres with enhanced visible light-induced photocatalytic oxidation performance for NO<sub>x</sub>, *Chemical Engineering Journal*, 406 (2021).
- [6] H. Wang, Y. Sun, G. Jiang, Y. Zhang, H. Huang, Z. Wu, S.C. Lee, F. Dong, Unraveling the mechanisms of visible light photocatalytic NO purification on earth-abundant insulator-based core-shell heterojunctions, *Environmental Science & Technology*, 52 (2018) 1479-1487.
- [7] K. Li, Y. He, P. Chen, H. Wang, J. Sheng, W. Cui, G. Leng, Y. Chu, Z. Wang, F. Dong, Theoretical design and experimental investigation on highly selective Pd particles decorated C<sub>3</sub>N<sub>4</sub> for safe photocatalytic NO purification, *Journal of Hazardous Materials*, 392 (2020) 122357.
- [8] J. Li, Q. Zhang, Y. Zou, Y. Cao, W. Cui, F. Dong, Y. Zhou, Ti<sub>3</sub>C<sub>2</sub> MXene modified g-C<sub>3</sub>N<sub>4</sub> with enhanced visible-light photocatalytic performance for NO purification, *Journal of Colloid and Interface Science*, 575 (2020) 443-451.